Electron-indium atom scattering and analysis of electron and optical spectra

Maja S Rabasović
Institute of Physics, Pregrevica 118 Belgrade, University of Belgrade, Serbia

E-mail: majap@ipb.ac.rs

Abstract. Experimental study of indium atom using electron and optical spectroscopy is presented in this paper. Both experimental techniques including experimental setups are described. Differential and integrated cross sections on elastic and inelastic electron scattering by indium atom are measured using electron spectrometer. The measurements are performed at incident electron energies of E0 = 10, 20, 40, 60, 80 and 100 eV within the large scattering angles ranging from 10° to 150° in steps of 10°. The experimental results are presented and comparison with the values predicted by calculated optical potentials method is conducted, showing good agreement. The differential cross sections (DCSs) for electron-impact excitation of the resonant state 6s 2S1/2 of Indium atom are measured at small and large angles. The forward scattering function method has been used for normalizing the generalized oscillator strengths (GOS) to determine optical oscillator strength and obtaining the absolute DCS values. Optical spectrum of In I and In II lines has been acquired by a streak camera. The experimental results regarding indium lines obtained by time resolved laser induced breakdown spectroscopy (LIBS) could be useful for obtaining the important plasma parameters such as temperature, electron density as well as plasma-expansion velocity and plasma starting times.

1. Introduction

Indium (atomic number 49) is the metallic element of group IIIa of the Periodic Table. It has open shell structure with the 5s2 5p configuration in the ground state. Term of the ground state according to Russell-Saunders coupling is 5p 2P1/2. The metastable (5p 2P3/2) and resonant (6s 2S1/2) levels are positioned at 0.274 and at 3.022 eV from the ground level, respectively.

Indium has a low melting point, 429.75 K. Owing to that indium is a very attractive in the production of semiconductor and optoelectronic devices. Indium oxide is a transparent ceramic material, when doped with Tin (~ 10%) it becomes conducting but stays transparent. Indium tin oxide (ITO) can be applied by coating to a wide range of glass and plastic materials to make transparent conducting panels [1, 2]. ITO is a part of each liquid crystal displays (LCD). Uses of indium are rapidly increasing, but on the other hand it is relatively rare material. It ranks the 61st in crustal abundance. It is about three times as abundant as silver.

Another very important role of indium is the application of an indium single ion as a reference for an optical frequency standard of the excellent stability and accuracy. The narrow 5s2 1S0 – 5s5p 3P0 transition in In+ at a wavelength of 236.5 nm could be used as a reference clock transition [3]. Further, indium is a suitable as a tracer for two line atomic fluorescence (TLAF) thermometry measurements [4]. This method works by using diode lasers based laser induced fluorescence with wavelength of 410

and 451 nm, respectively, to excite the temperature sensitive 5p 2P1/2 – 6s 2S1/2 and 5p 2P3/2 – 6s 2S1/2 transitions of indium atoms seeded into a flame.

Advantage of the indium atoms is that the split-orbit splitting in the 5p ground state of indium leads to an energy spacing that is equal to kT in typical combustion environments (1000-3000 K) [4]. Later, Chrystie et al [5] demonstrated the capability of this technique for time-resolved measurements in an acoustically perturbed flame.

In this paper we present experimental results obtained using electron and optical spectroscopy. The results that concern the elastic differential cross sections and resonant excitation of indium are obtained using electron spectroscopy in our laboratory [6, 7]. The other techniques that are implemented in our laboratory are based on laser induced phenomena (laser induced fluorescence and laser induced breakdown spectroscopy (LIBS)). The later mentioned is a type of optical emission spectroscopy that uses a highly energetic laser pulse to create a plasma plume on the sample surface [8]. At the end of the laser pulse, the plasma cools and excited ions and atoms emit characteristic optical radiation which could be used to analyze the spectral lines of the component in material [9, 10]. LIBS can detect all elements, limited only by the energy of the laser pulse as well as the sensitivity and wavelength range of the spectrograph and detector.

2. Experimental techniques

2.1. Electron spectrometer (ESMA)

A detailed description of the apparatus ESMA and has been given elsewhere [6, 7]. A crossed beam technique was exploited in electron spectroscopy measurements. Electron spectrometer ESMA consists of the hemispherical selectors in monochromator and analyser, the cylindrical lenses, the rotating plate on which the analyser is mounted and that provides assessment of scattering angles from -30° to +150° in respect to incident electron beam. Perpendicularly to the scattering plane defined by the incident and scattered view cones of the monochromator and analyser, the resistively heated oven is placed on together with the several layers of tantalum shields and copper shield in outermost radius as well as the copper cold finger cup for collecting metal atom vapours (Figure. 1(a)).

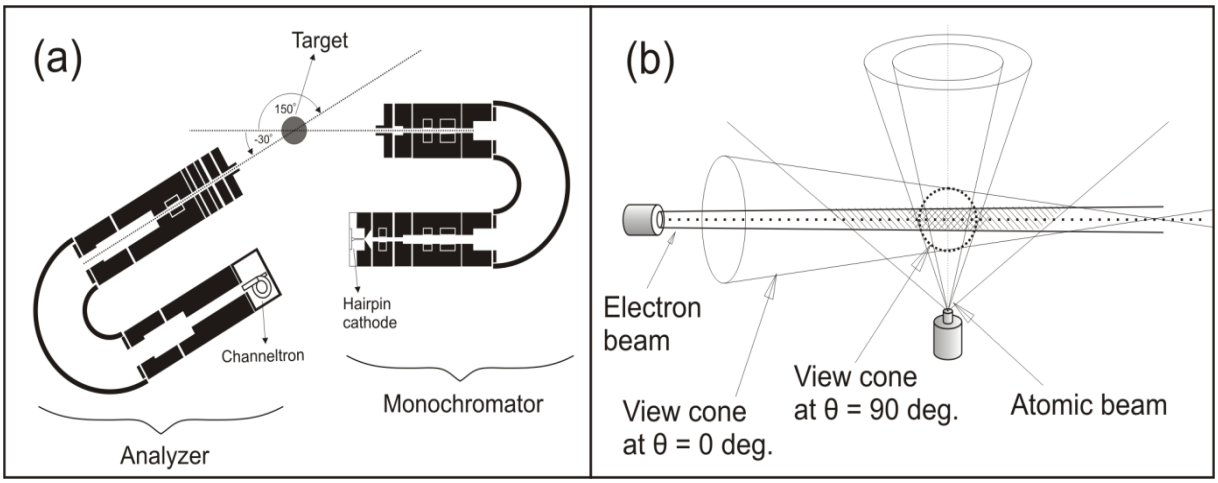

Figure 1. (a) Schematic overview of electro-optical system in spectrometer ESMA. **(b)** Scattering geometry in electron-atom beam experiments. The intersection of the indium atom beam, electron beam and view cone of the detector presents the interaction volume.

The indium vapour beam was produced by heating the oven crucible containing In metal. The oven has been modified in order to achieve higher temperatures. The oven consists of two separate heaters with the same diameters, one for the top of the stainless steel crucible and nozzle, and the other for the body of the crucible, and their temperatures were controlled by two thermocouples. The heating

currents of those heaters were 5.3 A and 3.4 A, respectively. They provided a variable temperature difference between the top and the bottom. The nozzle was maintained at approximately 100° higher temperature. The atomic beam was effused through a L = 20 mm long channel in the cap of the oven crucible that has an inner diameter of 2a = 2.5 mm. The aspect ratio was large (γ = 0.125). The evaporation temperature of the indium was approximately 1300 K and the metal-vapor pressure was about 10 Pa (0.07 Torr).

2.2. Time resolved LIBS system

The system for LIBS measurements consists of the excitation and detection parts. A schematic diagram of the experimental system is shown in Figure 2. Nd:YAG laser and Optical Parametric Oscillator (OPO, Vibrant 266) are used as the excitation part. The OPO system, pumped by a pulsed Q switched Nd:YAG laser (Briliant B) includes the second and fourth harmonic generator (SHG and FHG). In this paper the fundamental output at 1064 nm and pulse energy of 17 mJ is used to create an optical breakdown in ambient air. Focusing of the laser beam is obtained using lens with the focal length of 40 mm. The OPO system is controlled by OPOTEK software installed on PC.

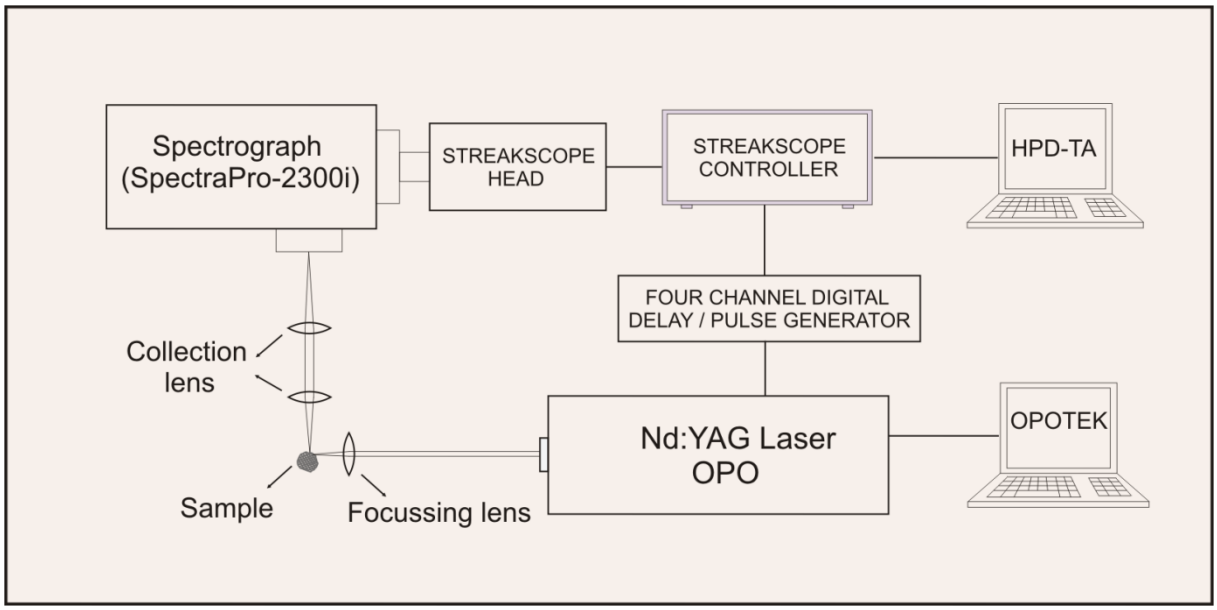

Figure 2. Time-resolved laser-induced breakdown: experimental setup.

The optical emission from the plasma plume is collected by using a spectrograph (SpectraPro 2300i) and recorded with a Hamamatsu streak camera (model C4334-01) with integrated video streak camera (Figure 3). The fundamental advantage of the streak camera is its two dimensional nature (wavelength and time), that is especially important in measuring time-resolved LIBS spectra. This enables monitoring of temporal evolution of the ionic and atomic emission lines or spatial development of the optical emission of the plasma plume. The data are acquired and analyzed using High Performance Digital Temporal Analyzer (HPD-TA) software, provided by Hamamatsu.

The spectrograph contains the triple grating turret. The diffraction gratings of 50, 150 and 300 g/mm were installed. For measurements presented in this paper the grating of 50 g/mm was used covering a 330 nm spectral range. The spectrograph was connected to the streak camera (Figure 3). In the streak camera, the light passing through the input slit is focused onto the photocathode of the streak tube by the input optics. The photocathode converts the light into photoelectrons that are accelerated by an electric field onto a phosphor screen. An electro-optical focusing system focuses the electrons on the screen. After passing the anode aperture the photo-electrons are deflected by a transversal electric field that increases linearly with time before reaching the phosphor screen. In this

way, the input spectra from different points of time are spatially separated on the phosphor screen. The phosphor layer converts the electrons into light that can be observed by a coupled CCD camera. The CCD chip has resolution of 640 x 480 pixels, and camera has the spectral range from 200 nm to 850 nm. Because the deflection of streak sweep is not completely straight, there is a geometric distortion of the streak image in the sweep direction, visible here as a tilted spectrum [11]. This distortion is easily removed by a curvature correction tool of the HPD-TA.

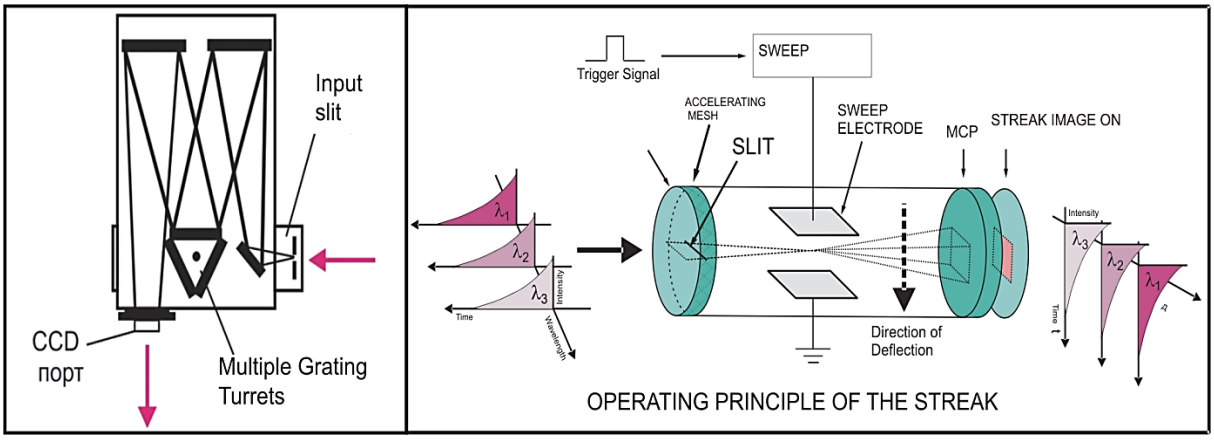

Figure 3. Schematic intersection of detection system (Spectrograph and streaktube).

3. Experimental results

3.1. Electron scattering by indium atom

We present experimental results regarding elastic electron indium atom scattering in the intermediate range. The results were presented and explained in detail in [6]. The measurements were performed at incident electron energies of E_0= 10, 20, 40, 60, 80 and 100 eV within the scattering angles ranging from 10° to 150°. Theoretical calculations have been carried out using the complex phenomenological optical potential (OP) with allowance of the spin-orbit interaction [6]. The real part of this potential without absorption is called the SEPSo approximation. The McCarthy type potential is used as the imaginary part of OP, which takes into account the absorption effects (SEPASo approximation). The relative values of experimental differential cross sections (DCSs) are normalized at 20° to the SEPASo theory. The three types of absorption potentials (VA_i , i=1, 2, 3) are used: two with summarized electron densities $\rho_1=\rho_{5p}+\rho_{5s}$ (VA_1) and $\rho_2=\rho_{5p}+\rho_{5s}+\rho_{4d}$ (VA_2) in subshells 5p, $5s^2$ and $4d^{10}$ and one with a partial influence of the electron density in $4d^{10}$ subshell (VA_3).

The comparison of the present experimental results with the present theoretical DCSs calculated in SEPSo and SEPASo approximations are presented in Figure 4. Note that at 10 eV and 20 eV, calculations with VA_1 and VA_3 coincide. As seen from Figure 4, the SEPSo calculation for all energies, except for 10 eV, reproduces the shape of the angular dependence of experimental cross sections, the number of minima and their angular positions. For 10 eV in theoretical calculations, as well as in the experiment, one minimum was obtained, but at 86°, that is about 20° shifted toward the lower angles than in the experimental DCS. For 40 eV and 60 eV DCS could be calculated using the absorption potential VA_1. At 80 eV and 100 eV the inclusion into absorption potential of the density ρ_{4d} (VA_2) gives a better agreement with the experimental data at intermediate and large scattering angles as compared to calculation using VA_1.

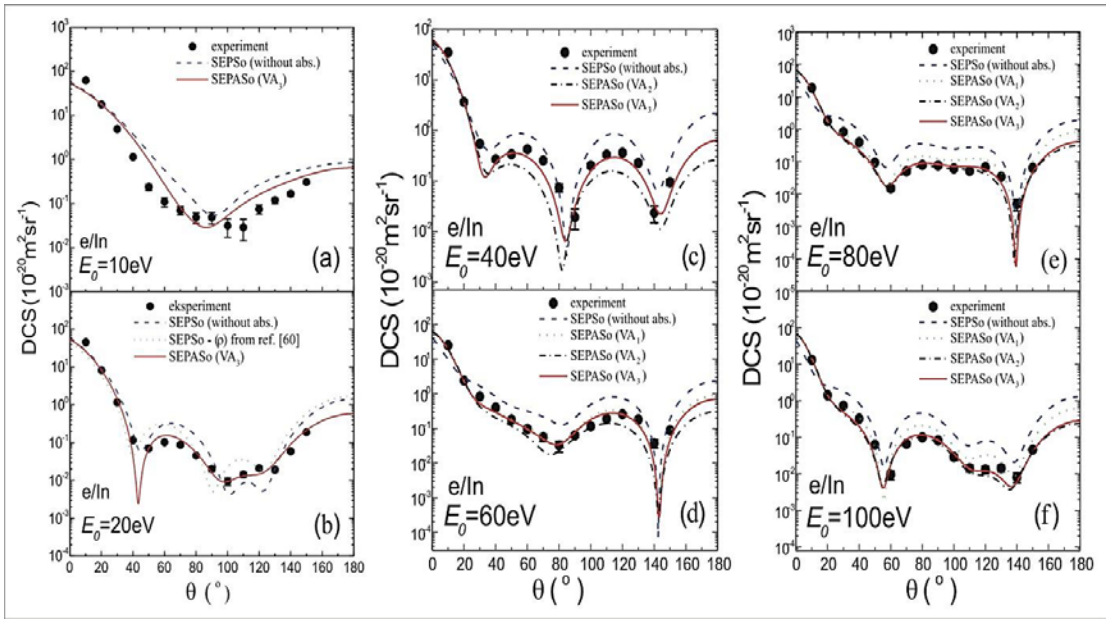

Figure 4. Differential elastic electron-indium atom scattering cross sections measured at 10, 20, 40, 60, 80 and 100 eV.

The experimental (circles) and theoretical (lines) results concerning the electron impact excitation of the resonant state 6s $^2S_{1/2}$ of indium atom are presented in Figure 5. We performed measurements for the electron-impact energies at 10, 20, 40, 60, 80 and 100 eV and at small scattering angles from 1° to 10° [7]. We normalized the relative DCSs by using the FSF method to absolute DCS values. Detailed explanation of this procedure could be seen in [7]. In Figure 5 we presented the absolute GOS values versus K^2 on a log-log graph together with the FSF for the resonant transition 5p $^2P_{1/2}$ – 6s $^2S_{1/2}$ in indium atom. The theoretical procedure was carried out within the framework of relativistic distorted-wave (RDW) calculations [12]. This RDW method is especially suited for the present study since it contains the effect of spin-orbit coupling for all the electrons in the system, both bound and free. In particular, the two fine structure levels of the ground state with separated wave functions and energy levels have been distinguished within the RDW method.

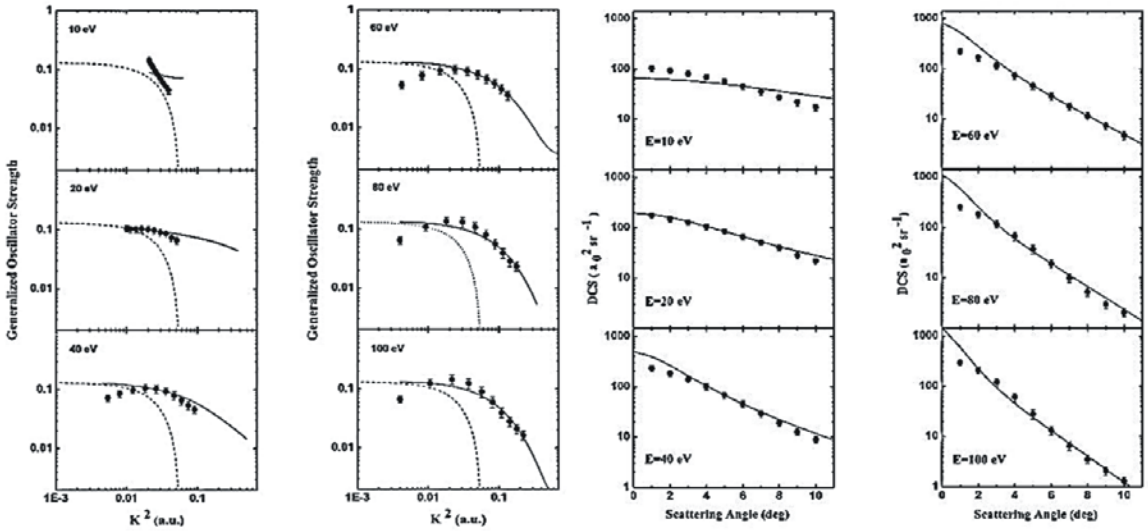

Figure 5. GOSs and DCSs for excitation of the resonant 6s 2S state of the indium atom at: 10 eV, 20 eV, 40eV, 60 eV, 80 eV and 100 eV electron-impact energies and at small scattering angles.

3.2. Optical emission spectra of indium using LIBS

A set of time resolved optical emission spectra for almost pure indium sample are presented in Figure 6. Time resolved measurements are performed in the time domain from 500 ns to 20 μs. In the early stage of laser induced plasma, the emission spectra are dominated by background continuum spectra due to bremsstrahlung radiation and recombination. The LIBS plasma obtained with nanosecond lasers exhibits a very intense continuum that decreases with time to allow detection of elemental emission. In order to reduce continuum it was utilized a delay unit for minimizing continuum to a reasonable level. Plasma shielding and subsequently the continuum emission could be reduced using lasers with femtoseconds or picoseconds pulse widths [13].

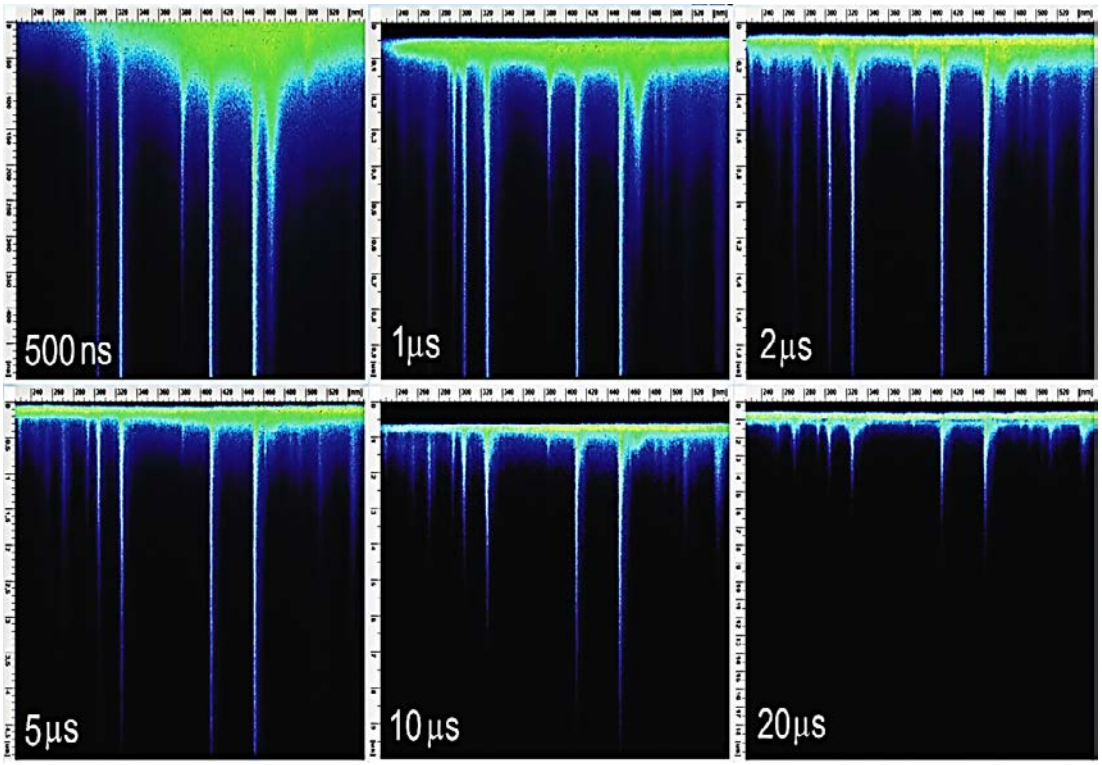

Figure 6. Time resolved LIBS streak images of pure indium sample with time range from 500 ns to 20 μs.

The temporal evolution of laser ablation plume from the image with time range of 1 μs (Figure 6) has been used for determination of the plasma parameters. We obtained the line profiles at 100 ns, 200 ns, 500 ns and 700 ns by the integration of the narrow range of time. From these profiles it can be seen how ionic lines (In II) dominate in the early stage of the plasma together with continuum radiation. Ionic lines are concentrated near the surface of the target. However, during cooling plasmas ionic lines are diminished while remaining the atomic (In I) lines as a result of recombination. The elemental analysis and plasma parameters (electron number density and electron temperature) could be determined from the emission spectra. The calculations show that both these parameters increase with the increase in the laser irradiance. The electron temperature (T_e) could be estimated using Boltzmann method or two lines method (271 and 451 nm) by assuming a local thermal equilibrium (LTE) and also that the plasma is optically thin (absorption and scattering can be neglected) [8, 10]. Electron temperatures obtained from line profiles in Figure 6 are typically ranged in the interval of 5000-20000K. The estimated electron density obtained using Saha Boltzmann equation amounts to ~ 10^{17} cm^{-3}. These values depend on the laser used and on the type of sample considered [10]. Variations of

the electron temperature and the electron density with the laser irradiance show that both these parameters increase with the increase in the laser irradiance [14].

4. Conclusions

In this paper were presented results regarding indium atom obtained by electron spectroscopy and laser induced breakdown spectroscopy. Possibility of detection of optically forbidden transitions is an advantage of electron spectroscopy. However, the resolution of our electron spectroscopy apparatus is lower than when using LIBS. The spectral lines obtained by electron spectroscopy can be combined with plasma emission measurements to select what emission lines could be used in the analysis. The possibilities of use of time resolved streak camera measurements may improve the analysis approach.

Analysis of streak images acquired using techniques explained here could be very useful for obtaining the important plasma parameters such as temperature, electron density as well as plasma-expansion velocity and plasma starting times, including their variation in time, or in the time frame of interest.

Acknowledgement

This work was financially supported within the Project of Ministry of Education, Science and Technological Development of the Republic of Serbia OI 171020

5. References

[1] Kuang Z, Perrie W, Liu D, Fitzsimons P, Edwardson S P, Fearon E, Dearden G and Watkins K G 2012 *Applied Surface Science* **258** 7601
[2] Fernandes S A Schoeps B Kowalick K, Nett R, Esen C, Pickshaus M and Ostendorf A 2013 *Physics Procedia* **41** 802
[3] Wang Y H Dumke R Liu T Stejskal A Zhao Y N Zhang J Lu Z H Wang L J Becker Th and Walther H 2007 *Optics Communications* **273** 526
[4] Hult J Burns I S Kaminski C F 2005 *Proceedings of the Combustion Institute* **30** 1535
[5] Chrystie R S M, Burns I S, Hult J and Kaminski C F 2009 *Optics Letters* **34** 2492
[6] Rabasovic M S Kelemen V I Tosic S D Sevic D Dovhanych M M Pejcev V Filipovic D M Remeta E Yu Marinkovic B P 2008 *Physical Review A* **77** 062713
[7] Rabasovic M S Tosic S D Sevic D Pejcev V Filipovic D M and Marinkovic B P 2009 *Nucl. Instrum. Meth. B* **267** 279
[8] D. Cremers and L. Radziemski 2006 *Handbook of Laser-Induced Breakdown Spectroscopy* John Wiley & Sons Ltd Chichester
[9] Vadillo J M and Laserna J J 2004 *Spectrochimica Acta Part B* **59** 147
[10] Milán M and Laserna J J 2001 *Spectrochimica Acta Part B* **56** 275
[11] Sevic D Rabasovic M S and Marinkovic B P 2011 *IEEE Transactions on plasma science* **39** 2782
[12] Das T Srivastava R Stauffer A D 2011 *Physics Letters A* **375** 568
[13] Miziolek A Palleschi V and Schechter I 2006 *Laser Induced Breakdown Spectroscopy* Cambridge University Press
[14] Shaikh N K Rashid B Hafeez S Jamil Y and Baig M A 2006 *J. Phys. D: Appl. Phys.* **39** 1384